

Structural and dynamical properties of Yukawa balls

D Block¹, M Kroll¹, O Arp¹, A Piel¹, S Käding², Y Ivanov², A Melzer²,
C Henning³, H Baumgartner³, P Ludwig³ and M Bonitz³

¹ IEAP, Christian-Albrechts-Universität, D-24098 Kiel, Germany

² Institut für Physik, Ernst-Moritz-Arndt-Universität, D-24098 Greifswald, Germany

³ ITAP, Christian-Albrechts-Universität, D-24098 Kiel, Germany

E-mail: block@physik.uni-kiel.de

Received 6 July 2007

Published 14 November 2007

Online at stacks.iop.org/PPCF/49/B109

Abstract

To study the structural and dynamical properties of finite 3D dust clouds (Yukawa balls) new diagnostic tools have been developed. This contribution describes the progress towards 3D diagnostics for measuring the particle positions. It is shown that these diagnostics are capable of investigating the structural and dynamical properties of Yukawa balls and gaining insight into their basic construction principles.

(Some figures in this article are in colour only in the electronic version)

1. Introduction

Ordered states of trapped charged particles are formed when the coupling parameter $\Gamma = Z^2 e^2 / 4\pi \epsilon_0 b k T$ exceeds a critical value, $\Gamma_{\text{crit}} \simeq 180$, for infinite systems. Here, Z is the charge number of the particles and b the interparticle spacing. In contrast to infinite systems, where usually body (bcc) or face-centered cubic (fcc) structures are the minimum-energy configurations, in finite systems the particles are arranged in a set of nested spherical shells. For example, in ion clusters ($Z = 1$, $b \approx 10 \mu\text{m}$, $T = 10 \text{ mK}$), such crystallized structures have been observed in simulations and experiments [1, 2]. In a dusty plasma, where highly charged microparticles ($Z \simeq 2000$) are trapped in a gas discharge, the regime of strong coupling is already entered at large interparticle distances ($b \approx 1 \text{ mm}$) and high temperatures ($T = 300 \text{ K}$). Additionally, dusty plasmas are highly transparent objects and the particle dynamics is sufficiently slow to observe individual particles and their dynamical properties by means of video microscopy. In the past, this has stimulated vivid research activities mainly on 2D dust systems. Recently, however, the 3D dust clouds have attracted more and more research activities. The 3D dust clouds have been studied under microgravity conditions [3, 4]. These clouds, however, usually suffer from dust-free regions (voids) in their center. The discovery of the formation of 3D finite spherical dust clouds under laboratory conditions without voids [5, 6]

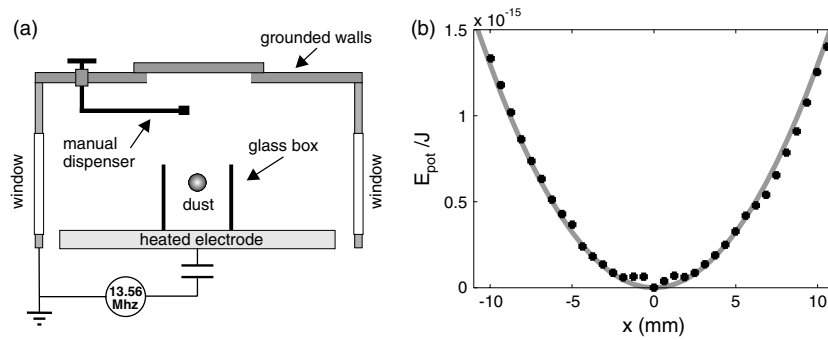


Figure 1. (a) A schematic cross section of the discharge chamber. The discharge is operated between the powered electrode and the grounded vacuum vessel. The dust particles are confined inside the upper half of the cubical glass tube, i.e. inside the bulk plasma region. The electrode is additionally heated to establish a temperature gradient and hence to exert an upward-directed thermophoretic force on the particles which compensates gravity. (b) Radial trap potential resulting from gravitational, electric and thermophoretic forces on a sample particle ($Q_d = 2000e$). The solid line is a parabolic fit to the experimental data (symbols) [7].

has opened up new possibilities to study the structural and dynamical properties of finite dust systems in detail.

This paper summarizes the progress in these so-called Yukawa balls. It addresses the problem of how Yukawa balls are generated and confined, summarizes their general structural properties and discusses the influence of screening on structure. For this purpose the recent developments of 3D diagnostics are reviewed and relations to other strongly coupled systems are discussed.

2. Generation and confinement

The experiments on Yukawa balls are conducted in a capacitively coupled rf-discharge at 13.56 MHz in argon in a pressure range 70–100 Pa. The discharge arrangement consists of a powered circular disc electrode of 15 cm diameter and the grounded vacuum vessel acts as a reference electrode (figure 1(a)). In addition, a glass tube with squared cross section is placed right at the center of the powered electrode. The discharge is operated at low rf-power ($P_{\text{rf}} < 10$ W) resulting in a peak plasma density of $n = 7 \times 10^{14} \text{ m}^{-3}$. The dielectric glass box accumulates negative surface charges which generate radial electric fields. These inward-directed electric fields provide a stable radial confinement for charged dust particles. To compensate for the dominant gravitational force in the vertical direction, the electrode is heated to typically 60 °C. The resulting temperature gradient in the neutral gas background between the ‘hot’ electrode and the ‘cold’ vacuum vessel yields an upward directed thermophoretic force, which is strong enough to compensate gravity. The combined action of radial electric fields, gravity and thermophoresis gives a stable isotropic confinement for the dust particles in the bulk plasma. The radial profile of this confinement potential is plotted in figure 1(b). The solid line is a parabolic fit to the experimental data [7]. Thus, this plasma trap has a harmonic trapping potential similar to a Paul trap for the confinement of laser-cooled ions.

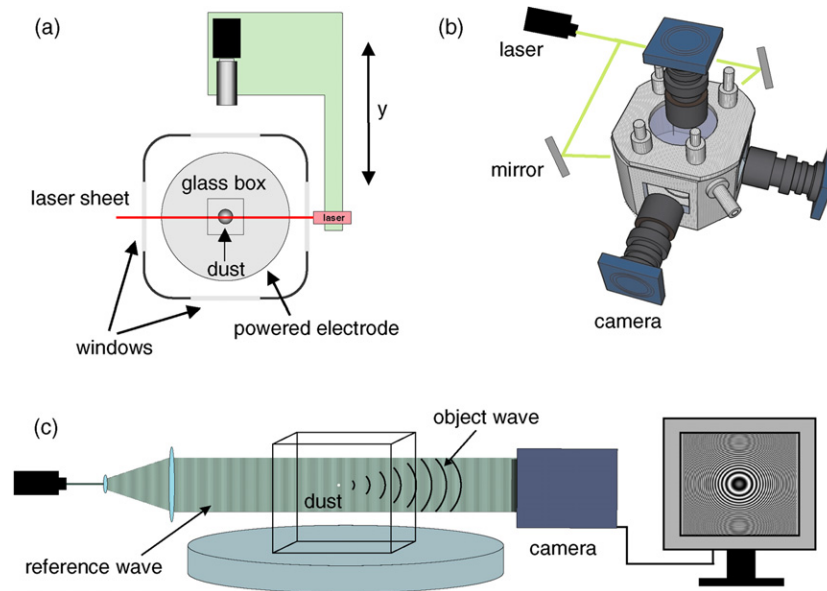


Figure 2. (a) Top view of the SVM setup. A vertical laser sheet illuminates a thin slice of the dust cloud. Images are taken at a right angle by a CCD camera with a macro lens. Camera and laser are mounted on a common translational stage to image all slices of the dust cloud during a scan. (b) The stereoscopic imaging setup consists of three cameras with a perpendicular optical axis. The dust cloud is illuminated from two sides with an expanded laser beam. (c) Setup for DIH. The expanded laser beam is the reference wave and interferes with the object wave at the CCD sensor. An interference pattern for a single particle is sketched on the monitor.

3. Diagnostics

To study these trapped dust particles (Yukawa balls), diagnostic methods are required which allow us to determine the position in 3D with high accuracy. In the following three developments and their characteristics are described: The scanning video microscopy (SVM), a stereoscopic imaging system (SIS) and digital inline holography (DIH).

3.1. Scanning video microscopy

SVM basically consists of a standard video microscope. The particles are illuminated with a laser sheet and their scattered light is detected with a CCD camera at right a angle (figure 2(a)). In addition, the camera and the laser are mounted on a translation stage. By moving the translation stage a sequence of slices of the trapped dust cloud is illuminated and recorded. Using a thin laser sheet ($d < 200 \mu\text{m}$) a series of slices of the Yukawa ball is observed. While the vertical (z) and the horizontal positions (x) of the particle are directly accessible in an image, the depth information is retrieved from the position of the translation stage and the brightness of the particle images in the neighboring slices. With this method, the 3D particle position can be recovered with an accuracy of about $\Delta x, y, z \approx 20 \mu\text{m}$. Although this diagnostic setup is simple and allows us to cover volumes of the order of cm^3 , the sequential image recording limits its use to static particle configurations, i.e. crystalline states. Further, it is to be noted that this technique requires careful calibration to obtain the particle position in absolute units. Nevertheless, it serves well to study the basic structural properties of Yukawa balls (see section 5 and [5, 7, 8]).

3.2. Stereoscopic imaging

A simultaneous determination of dust particle positions can be achieved if the particle cloud is observed with at least two cameras from different perspectives [10, 18]. Such a SIS is sketched in figure 2(b). In our experiments, three cameras with perpendicular optical axes are used to image the volume around the intersection of their optical axes. The particles are illuminated by two expanded laser beams and the scattered light of the particles is observed in forward scattering to maximize the brightness of the particle images. The resolution of SIS is comparable to those of SVMs and the frame rate $f > 100$ fps allows us to study fast dust dynamics, e.g. even the thermal fluctuations of the particles around their equilibrium positions' motion. Due to the aperture of the lens systems the focal depth of each camera is limited to about 3 mm, which implies that presently only small dust clouds with $N \leq 100$ particles are accessible with SIS. The advantage of using three cameras is that each particle is visible at least in one pair of camera images. This allows the unambiguous determination of the 3D position of all particles even if the particle images overlap in one camera image. However, with a higher particle number in the Yukawa ball an unambiguous position reconstruction becomes increasingly difficult. For larger systems, lens aberrations have to be taken into account for position reconstruction. This requires a careful calibration of the system and sophisticated reconstruction algorithms. However, for small dust clouds, SIS works very well and typical results of the system are given in section 6.

3.3. Digital holography

The generic problem of a small focal depth of SVM and SIS is caused by the aperture of the lens systems. Thus, it is tempting to find a way to record a particle cloud without lenses, namely; the DIH. The basic DIH setup is depicted in figure 2(c). It consists of a laser and a beam expander on the entrance side of the dust cloud and the CCD sensor on the exit side. The CCD sensor records the interference pattern of the reference wave (laser) and the object wave, consisting of light scattered by the dust particles. By numerical deconvolution of the resulting interference pattern on the CCD chip the 3D dust positions can be reconstructed from the recorded digital hologram. First results show that it is possible to record digital holograms of dust clouds immersed in a plasma environment and to successfully reconstruct the dust cloud. So far, the accuracy of particle positions is about $\Delta y < 100 \mu\text{m}$ in depth and $\Delta x = \Delta z = \pm 20 \mu\text{m}$ in the perpendicular plane, but further refinements of the setup and the reconstruction scheme promise a reduction of Δy . It should be noted that the accessible volume is comparable to that of SVM, that this method does not require any calibration and that no shadowed positions exist. Therefore, DIH promises to be a suitable method for extended dust clouds. However, the read-out time of the large sensor (4 Mpixel) limits the temporal resolution and the holographic recordings are not suitable for online monitoring.

4. Molecular-dynamics (MD) and monte-carlo (MC) simulations

Many results for dusty plasmas have shown that the influence of the plasma on the dust can be reduced to a static Debye screening and a simple constant charging of the dust grains. This allows us to study the few-particles dust system by means of MD and MC simulations using the Hamiltonian

$$H = \sum_{i=1}^N \left\{ \frac{p_i^2}{2m} + \frac{m\omega^2}{2} r_i^2 \right\} + \sum_{i>j} \frac{Q^2}{4\pi\epsilon_0 r} \exp(-r/\lambda_D) \quad (1)$$

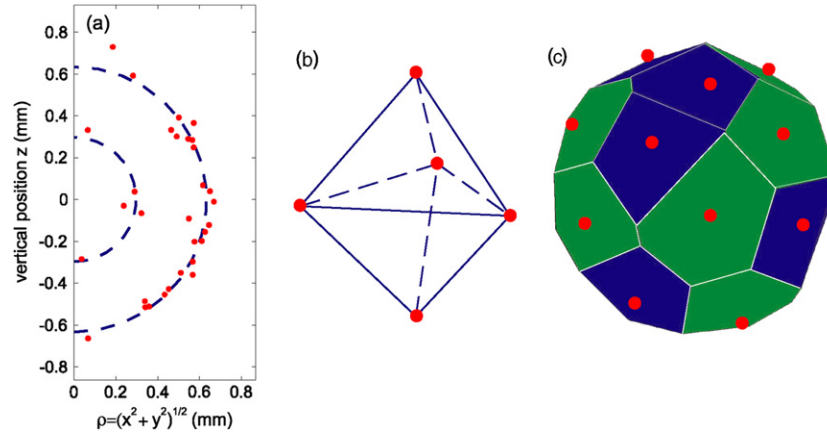


Figure 3. Structure of a $N = 31$ cluster. (a) Particle positions in cylindrical coordinates in the ρ - z plane. The red dots are the average particle positions of a (5,26) configuration. The dashed lines indicate the shell radii. (b) Structure of the inner shell. (c) Voronoi analysis of the corresponding outer shell with $N_o = 26$. Pentagons are black (blue) and hexagons are gray (green). The particle positions are marked with dots. All plots show experimental results.

with a harmonic confinement potential and a Yukawa-type pair potential. These simulations are ideal tools to study parameter dependences and analytical descriptions which are not easily accessible in experiment. For the comparison of experiments and simulation it is important to notice that the experimental data and the simulation output are both time-dependent particle positions. Therefore, identical tools can be used in both cases for data evaluation and a direct comparison of simulation and experiment is possible, as we will show in the following sections.

5. Structural properties

Using the diagnostics introduced in section 3, it is possible to investigate the structure of Yukawa balls recorded with SIS. Figure 3(a) visualizes the typical structure of a Yukawa ball. Using cylindrical coordinates z and $\rho = \sqrt{x^2 + y^2}$ only, a clear formation of shells is observed. On the inner shell 5 particles are found and 26 particles form the outer shell. While the inner shell is a symmetric double-tetrahedron (figure 3(b)) and represents a typical closed-packed structure, the outer shell and its Voronoi analysis [11] show a pattern of hexagons and pentagons (figure 3(c)), i.e. the same very regular particle arrangement one expects if a 2D hexagonal lattice is bent to a sphere. Repeating this type of analysis for about 50 clusters consisting of 100 to 500 particles, which are recorded by SVM [8, 19], reveals that the shell structure with its hexagonal lattice with pentagonal defects is the generic structure of Yukawa balls. Furthermore, the intershell distance d is found to be $d = 0.86b$, where b is the particle distance on the shell. This is in excellent agreement with the local icosahedral ordering [1]. Therefore, Yukawa balls are crystals which show the same type of structure as, e.g. laser cooled ions [1, 2, 12]. Moreover, the structural properties are fully reproduced in MD and MC simulations [8, 9, 13]. Further, the so-called magic configurations, i.e. very stable clusters due to closed shell configurations, are similar to those arising from pure geometric considerations only [13, 14]. Hence, the structural properties of Yukawa balls are governed by geometrical constraints.

Nevertheless, the structure of Yukawa balls is not identical to those of pure Coulomb systems. While laser-cooled ions are pure Coulomb systems, the particle interaction in Yukawa

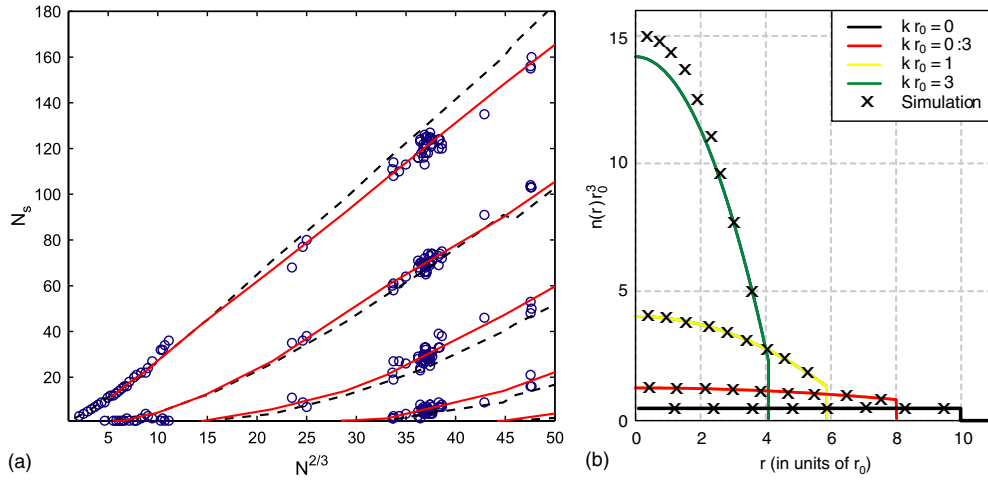


Figure 4. (a) Experimental (symbols) and simulation (lines) results for the shell population of three-dimensional Coulomb clusters. The dashed line marks the simulation results for unscreened Coulomb interaction of the particles. The solid line results from simulations with a screening parameter $\kappa r_0 = 0.6$. r_0 is the stable distance of two particles in the absence of screening. (b) Radial density profiles obtained from a fluid model for different screening parameters [15]. The results of MD-simulations are marked by symbols. Note that the density profile for an unscreened system is constant while screening introduces a radial density gradient.

balls is weakened by screening. The effect of screening on the structure becomes evident if the shell occupation number is studied as a function of the cluster size for a Coulomb and a Yukawa system (figure 4(a)). Compared with the Coulomb case, a Yukawa system contains fewer particles in the outer shells while the population of the inner shells is enhanced. Starting from a homogeneous density profile in a Coulomb system [15], an increase in the screening strength thus results in a radially inhomogeneous density profile (figure 4(b)). This result is fully consistent with predictions from a fluid model [15, 16] and even holds for small systems ($N < 100$) if the statistical distribution of metastable configurations of clusters is taken into account [17].

This structural change is the consequence of the range of the particle interaction and the particle distribution. In a Coulomb system, the net force on a particle inside a homogeneously charged shell is zero because the shell surface, and hence the charge seen at a certain solid angle, scales with $Q \sim r^2$ while the Coulomb force goes with $F_C \sim r^{-2}$. This means that inner shells in a Coulomb system do not experience a force from the outer shells. However, when screening is present and the nearest-neighbor interaction becomes dominant, a particle on an inner shell feels a radially inward directed force. Therefore, a local force equilibrium for a shell configuration can be obtained only if the radially inward-directed force is compensated by additional charges (i.e. particles) on inner shells. The result is a radial density gradient, as observed in experiment [8, 17] and predicted by the fluid model [15, 16].

6. Dynamical properties

With SIS, we are able to study the dynamical properties of Yukawa balls. The thermal motion of the particles, for example, can be used to study the normal mode spectrum of a cluster in order to investigate their stability or deduce important system parameters such as the particle

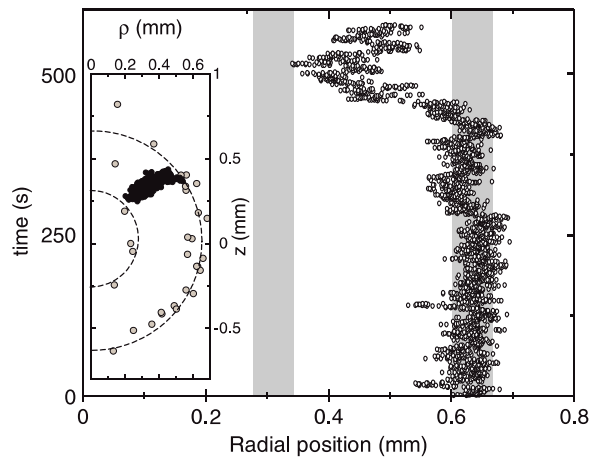


Figure 5. Shell transition in a cluster with $N = 31$ particles. The configuration changes from (4,27) to (5,26). The radial component of the trajectory of the particle leaving the outer shell is plotted in the main panel. The average radial positions of the other particles are indicated by the shaded regions (shells). The inset shows the particle trajectory in the ρ - z plane (black symbols) and the average position of the other particles (open symbols).

charge or the screening length [18]. Another interesting subject is phase transitions in finite systems in particular as they can be studied on a kinetic level in Yukawa balls. The onset of such phase changes are transitions between (metastable) configurations. An example of such a transition between two shell configurations is shown in figure 5. The inset in figure 5 depicts the shell configuration of a $N = 31$ cluster. While most particles remain on their shell (their average position is indicated by open symbols) one particle leaves the outer shell and approaches the inner shell. The time dependence of its radial position is also shown in figure 5. Before the particle moves radially inwards, just the thermal motion of the particle around the equilibrium position in the outer shell is observed. The amplitude of the thermal motion in the radial direction already indicates that this Yukawa ball is near the solid–fluid phase transition. At $t = 400$ s, the particle leaves the outer shell and approaches the inner shell where it stays for a short while before it returns to the outer shell. This observation demonstrates that the full particle dynamic is accessible in experiment and that the thermal energy of the particles is sufficiently large to populate metastable states and finally to study the phase transitions at a microscopic level.

7. Summary and conclusions

To summarize, since the discovery of Yukawa balls the development of new diagnostics in combination with dedicated simulations has led to considerable progress in the understanding of the structural properties of finite 3D strongly coupled systems. Besides the characteristic shell structure with hexagonal order on the shells, it was possible to show that screening influences the radial structure of finite clusters of all sizes. Based on the good agreement of the results in experiment, simulation and theory, it was demonstrated that the range of the particle interaction is responsible for these changes. An important result is that Yukawa balls have many similarities with other finite strongly coupled systems. Due to their unique experimental properties, Yukawa balls will allow us to study waves, phase transitions and thermodynamic properties at a kinetic level. The new 3D diagnostic systems SIS and DIH have already demonstrated that these types of experiments are feasible.

Acknowledgment

Financial support by Deutsche Forschungsgemeinschaft via SFB-TR24 grants A2, A3, A5 and A7 is gratefully acknowledged.

References

- [1] Hasse R W and Avilov V V 1991 *Phys. Rev. A* **44** 4506
- [2] Mortensen A, Nielsen E, Matthey T and Drewsen M 2006 *Phys. Rev. Lett.* **96** 103001
- [3] Morfill G E, Thomas H M, Konopka U, Rothermel H, Zuzic M, Ivlev A and Goree J 1999 *Phys. Rev. Lett.* **83** 1598
- [4] Morfill G E, Thomas H M, Annaratone B M, Ivlev A, Quinn R A, Nefedov A P and Fortov V E 2002 *AIP Conf. Proc.* **649** 91
Morfill G E, Thomas H M, Annaratone B M, Ivlev A, Quinn R A, Nefedov A P and Fortov V E 2002 *AIP Conf. Proc.* **649** 507
- [5] Arp O, Block D, Piel A and Melzer A 2004 *Phys. Rev. Lett.* **93** 165004
- [6] Annaratone B M, Antonova T, Goldbeck D D, Thomas H M and Morfill G E 2004 *Plasma Phys. Control. Fusion* **46** B495
- [7] Arp O, Block D, Klindworth M and Piel A 2005 *Phys. Plasmas* **12** 122102
- [8] Bonitz M, Block D, Arp O, Golubnychiy V, Baumgartner H, Ludwig P, Piel A and Filinov V 2006 *Phys. Rev. Lett.* **96** 075001
- [9] Baumgartner H, Kählert H, Golubnychiy V, Henning C, Käding S, Melzer A and Bonitz M 2007 *Contrib. Plasma Phys.* **47** 281–90
- [10] Käding S and Melzer A 2006 *Phys. Plasmas* **13** 090701
- [11] Barber C B, Dobkin D P and Huhdanpaa H T 1996 *ACM Trans. Math. Softw.* **22** 469–83
- [12] Dubin D H E and O’Neill T M 1999 *Rev. Mod. Phys.* **71** 87
- [13] Ludwig P, Kosse S and Bonitz M 2005 *Phys. Rev. E* **71** 046403
- [14] Mackay A L 1962 *Acta Cryst.* **15** 916
- [15] Henning C, Baumgartner H, Piel A, Ludwig P, Golubnychiy V, Bonitz M and Block D 2006 *Phys. Rev. E* **74** 056403
- [16] Henning C *et al* *Phys. Rev. E* at press
- [17] Block D *et al* *Phys. Rev. Lett.* submitted
- [18] Käding S, Ivanov Y and Melzer A 2007 *IEEE Trans. Plasma Sci.* **35** 328
- [19] Block D, Arp O, Piel A and Melzer A 2006 *AIP Conf. Proc.* **862** 203